Research Report

Establishment of Real-Time Multispectral Imaging for the Detection of Bladder Cancer Using a Preclinical in Vivo Model

Sabine Meessen[a,1], Jan Rother[b,1], Xi Zheng[a], Markus Eckstein[c], Maximilian C. Kriegmair[d], David Hernandez[b], Bartłomiej Grychtol[b,e], Nikolaos C. Deliolanis[b,e], Christian Bolenz[a,*] and Cagatay Günes[a,*]

[a]*Department of Urology, Ulm University, Ulm, Germany*
[b]*Medical Faculty Mannheim – Heidelberg University, Mannheim, Germany*
[c]*Department of Pathology, University Hospital Erlangen, Erlangen, Germany*
[d]*Department of Urology, University Medical Center Mannheim, Mannheim, Germany*
[e]*Fraunhofer IPA, Project Group for Automation in Medicine and Biotechnology, Mannheim, Germany*

Abstract.
BACKGROUND: Emerging imaging technologies such as real-time multispectral imaging (rMSI) hold great potential for simultaneous visualization of multiple target structures using fluorophores on various tumours including bladder cancer (BC). These technologies, however, require a multi-step preclinical evaluation process, including mouse models.
OBJECTIVE: To demonstrate the suitability of the new rMSI technology for the detection of premalignant lesions and malignant BC in a preclinical mouse model using contrast agents.
METHODS: Tumours were induced by N-butyl-N-(4-hydroxybutyl)-nitrosamine (BBN), which is known to induce BC in rodent models. In total, 30 mice (C57BL/6) were fed with 0.1% BBN *ad libitum* in drinking water for up to 5 months. Bladders were excised at 3 ($n = 6$) and 5 months ($n = 24$) of treatment and incubated *ex vivo* with Hexaminolevulinat (HAL, Hexvix®), CD47-FITC, CD90.2-FITC or a combination of CD90.2-FITC/CD47-FITC and HAL. The bladders were analyzed by an endoscopic rMSI prototype system equipped with a spectral filter (Chroma), a 4 mm endoscope (Karl Storz) with 30° optic, a LED light source and a PC with a microcontroller board.
RESULTS: 5-month treatment of mice with 0.1% BBN led to the formation of squamous carcinoma (46%, $n = 11$) while urothelial carcinoma was observed only in one mouse (4%, $n = 1$). Carcinoma *in situ* (CIS) was detectable in twelve out of twenty-four mice (50%, $n = 12$) treated for 5 month and in three out of six mice (50%, $n = 3$) treated for 3 months. The metabolite of HAL, protoporphyrin IX (PpIX), could be reliably and specifically detected in all of mouse bladder tumours and CIS. However, detection of the CD90.2 surface marker was less reliable, potentially due to species- or tumour-subtype specificity.

---

[1]Equal contribution.

*Correspondence to: Prof. Dr. Cagatay Günes, Department of Urology, Ulm University, Helmholtzstr. 10, 89081 Ulm, Germany. Tel.: +49 0 731 500 58019; Fax: +49 0 731 500 58093; E-mail: cagatay.guenes@uniklinik-ulm.de and Prof. Dr. Christian Bolenz,

Department of Urology, Ulm University, Albert-Einstein-Allee 23, 89081 Ulm, Germany. Tel.: +49 0 731 500 58000; Fax: +49 0 731 500 58002; E-mail: christian.bolenz@uniklinik-ulm.de.

CONCLUSIONS: This model offers the potential for preclinical imaging studies with combined fluorescence targets, e.g. HAL, in combination with BC-specific antibodies.

INTRODUCTION

Bladder cancer (BC) is one of the most common cancers with significant medical and economic implications [1, 2]. Nearly 70% of BCs are non-muscle invasive tumours at diagnosis and are treated with repeated endoscopic resection and instillation therapies [3]. Tumour recurrence and progression to invasive BCs are the major challenges in BC therapy [4]. Reliable detection of early-stage or recurrent BC would improve therapy options. Currently, detection of bladder tumours mainly relies on the accuracy of white light cystoscopy (WLC) [5]. However, WLC has several limitations, including difficulties with flat lesion detection, precise tumour delineation for complete resection, and grade and stage determination. Each limitation concurs with surgeon skills and experience with the available technology for visualization and resection.

In the last decade, more sophisticated detection methods have been developed, including fluorescence cystoscopy/photodynamic diagnosis, narrow-band imaging, confocal laser endo-microscopy, and optical coherence tomography, which address the limitations of WLC. The new techniques allow detection of suspicious lesions (photodynamic diagnosis and narrow-band imaging) and help to characterize the lesions (optical coherence tomography and confocal laser endo-microscopy) [6–8]. Photodynamic detection (PDD) proved to be superior over WLC for detection of flat lesions and up to 40% of carcinoma *in situ* can only be identified with PDD-imaging [9]. One major limitation of the currently available imaging modalities is that simultaneous application or combination with white light is impossible.

We have recently established a separate visualization of multiple spectral components using real-time multispectral imaging (rMSI) [10]. The system consists of a camera head with a special filter, a control unit and a multi-LED light source. The technology is based on a spectral and temporal multiplexing scheme for simultaneous imaging of (white light) reflectance and fluorescence from multiple fluorophores e.g. protoporphyrine IX (PpIX) or fluoresceine in real-time and video rate. Using unmixing algorithms it is possible to separate the spatial distribution of single fluorophores. The rMSI system also allows to display chromoendoscopic modalities similar to narrow band imaging (NBI). Thus, combinations of these modilities can be merged into a single image, which is a great advantage in clinical practice, as the current standard procedure of manual switching between fluorescence modalities and (white light) reflectance becomes obsolete. With the rMSI system, the surgeon is able to observe the distribution of fluorophores, which, for instance, specifically marks cancerous tissue (e.g. by PpIX) while he can navigate and resect under white light conditions at the same time. In a pilot study, we adapted the rMSI system for urethrocystoscopy that allowed visualization and combination of up to five imaging modalities [11].

In the present study, we aimed to establish a preclinical animal model to develop the rMSI device further and to expand its clinical application. For this purpose, the BBN-induced mice bladder tumours are incubated *ex vivo* with 5-ALA (5-aminolevulinic acid) only and/or with two antibodies (CD47 and CD90.2, respectively) which are highly expressed in human BC [12–14] in combination with white light. Our results indicate that the new rMSI device is suitable for tumour detection with HAL and image combination with white light. Importantly, in addition to invasive bladder tumours, we could also detect carcinoma *in situ* in the mouse bladder.

MATERIALS AND METHODS

BBN-induced carcinogenesis

Male C57BL/6JRj mice were obtained from Janvier Labs (Janvier Labs, France). Mice received 0.1% BBN (Sigma Aldrich Biochemie GmbH, Hamburg, Germany. Cat.-Nr. B8061*) ad libitum* in drinking water for 3 ($n = 6$) or 5 ($n = 24$) months. The drinking water containing BBN was prepared once a week. The experiments were conducted with the approval of the Baden Württemberg animal ethics committee (animal experiment number: 1326). Mice were sacrificed, and bladders were prepared for *ex vivo* detection of tumours by rMSI. Hexaminolevulinat (HAL), CD90.2-FITC (Miltenyi Biotec B.V. & Co. KG, Bergisch Gladbach, Germany), CD47-FITC (BD

Biosciences, San Jose, CA, USA), CD47-FITC/HAL combinations and CD90.2-FITC/HAL combinations were directly applied on the mouse tumours. Five non-treated control mice (no BBN-treatment, normal urothelium) and 30 BBN-treated mice were analyzed. For histopathological visualization 2 μm thick whole slide section of each FFPE block were cut, mounted on conventional STARFROST glass slides and stained with Hematoxylin and Eosin (HE).

Preparation of murine bladders for imaging with the multispectral camera system

The bladders were incubated for 1 hour in 8 mM HAL (Sigma-Aldrich Biochemie GmbH, Hamburg, Germany) and different concentrations (1 μg/ml – 4 μg/ml) of FITC-labelled antibodies against CD47 (BD Biosciences, San Jose, CA, USA), or CD90.2 (Miltenyi Biotec B.V. & Co. KG, Bergisch Gladbach, Germany) in DMEM (ThermoFisher, Paisley, Scotland) containing 15% FCS (Sigma Aldrich, Steinheim, Germany), 1% Penicillin/Streptomycin (PAN-Biotec GmbH, Aidenbach, Germany), 5% Glutamax (ThermoFisher, Grand Island, New York, USA), 1% non-essential aminoacids (ThermoFisher, Paisley, Scotland) and 1% sodium pyruvate (Life Technologies Europe BV, Bleiswijk, Netherlands). The bladders were fixed onto a cork, which was painted black with a permanent marker, glued into a 12-well plate (Sarstedt AG & Co. KG, Nürnbrecht, Germany) using a double-sided scotch tape. For imaging, the bladder was immersed into DPBS (Lonza Group Ltd, Basel, Switzerland).

Multispectral imaging of excised mouse bladders

The general principle of the multispectral camera system is described elsewhere [6]. Briefly, the camera system consists of a USB camera (Ximea GmbH, Münster, Germany) with a custom-designed filter (Chroma Technology Cooperation, Bellows Falls, VT, USA), a video adapter (R.Wolf, Knittlingen, Germany), a microcontroller unit, a multi-LED light source (Omicron-Laserage Laserprodukte GmbH, Rodgau, Germany), and a PC for data acquisition. For imaging of the specimens, a 4 mm 30° endoscopy optic and a liquid light guide were used (Karl Storz GmbH, Tuttlingen, Germany). The white light images and the fluorescence images of murine bladders were acquired concurrently and saved as uncompressed 16-bit tif-images with bayer pattern (raw-image format).

Image/video processing

The image processing was performed using Python and OpenCV. All images were background corrected, transformed to RGB, colour corrected and gamma corrected. Additionally, a simple intensity-based threshold was used for masking the data. The fluorescence data were unmixed into a PpIX fluorescence channel and a background fluorescence channel, which combined tissue autofluorescence and fluorescein fluorescence from labelled antibodies, using matrix multiplication. The ratio of PpIX and BGD fluorescence highlighted areas with high PpIX fluorescence. For quantification 100 sequential images were selected, and the median value of the PpIX and BGD ratios were calculated for each frame. The median value of the 100 frames was calculated yielding a single value per mouse bladder. The statistical analysis was performed using the python library scipy.stats (https://docs.scipy.org/doc/scipy/reference/stats.html).

Evaluation of the signal intensity was done by visual inspection of the processed videos. The signal intensity for a bladder was rated 1.0 (strong), 0.5 (moderate), 0.25 (weak), 0.125 (very weak), and 0 (no signal, see also Table 1).

RESULTS

BBN-induced bladder cancer recapitulates human BC

We used the established N-butyl-N-(4-hydroxy butyl)-nitrosamine (BBN) bladder cancer (BC) model to induce tumours [15, 16] administrating 0.1% BBN *ad libitum* (Fig. 1A). BBN specifically induced tumours in the bladder, resulting in the development of invasive tumours by five months. Recent studies demonstrated that the tumours substantially reflect morphological and molecular characteristics of human BC [17–19].

Histological evaluation of mice bladder tissue revealed that 50% (12 of 24) of the 5-months BBN-treated mice develop invasive BC (defined as cancer cells invading the submucosal tissue layer or the muscularis propria) (Figs. 1B–D). As reported earlier, the majority of these tumours are of basal origin and represent squamous cell carcinoma (SCC) (Table 1). Moreover, 17% (4/24) of the five months BBN-treated mice exhibit carcinoma *in situ* (CIS) with focal invasion, and 33% (8 of 24) developed CIS. On the other hand, none (0/6) of the three months

Table 1
Semi-quantitative evaluation of PpIX signals in relation to tumour histology

Mouse Number	Pathology	PpIX Signal Intensity	PpIX signal (yes or no)
BBN-treated (5 months) +HAL			
1	Urothelial Carcinoma	0,5	yes
2	Squamous Carcinoma	1	yes
3	Squamous Carcinoma	0,5	yes
4	Squamous Carcinoma	0,25	yes
5	Squamous Carcinoma	0,5	yes
6	Squamous Carcinoma	0,25	yes
7	Squamous Carcinoma	1	yes
8	Squamous Carcinoma	0,25	yes
9	Squamous Carcinoma	0,25	yes
10	Squamous Carcinoma	1	yes
11	Squamous CIS with focal invasion	0,25	yes
12	Squamous CIS with focal invasion	0,5	yes
13	Squamous CIS with focal invasion	0,5	yes
14	Squamous CIS	1	yes
15	Squamous CIS	0,25	yes
16	Squamous CIS	0,5	yes
17	Squamous CIS	1	yes
18	Squamous CIS	0,5	yes
19	Squamous CIS	0,25	yes
20	Squamous CIS	0,25	yes
BBN-treated (3 months) +HAL			
1	Squamous CIS	0,125	yes
2	Squamous CIS	0,125	yes
3	Squamous CIS	0,25	yes
4	Squamous Metaplasia	0,25	yes
5	Squamous Metaplasia	0	no
6	Squamous Metaplasia	0	no
BBN-treated (5 months) w/o HAL			
1	Squamous Carcinoma	0	no
2	Squamous CIS with focal invasion	0	no
3	Squamous CIS	0	no
4	Squamous Carcinoma	0	no
untreated + HAL			
1	normal epithelium	0,125	yes
2	normal epithelium	0	no
3	normal epithelium	0	no
4	normal epithelium	0	no
5	normal epithelium	0	no

PpIX signal intensity: 1, strong signal; 0.5, moderate signal; 0.25, weak signal; 0.125 very weak signal and 0 no signal.

BBN-treated mice developed macroscopic lesions (Figs. 1B–D). While CIS could be observed in 50% of these mice (3/6), the other 50% (3/6) showed focal metaplasia (Fig. 1C, D). As expected, none of the control mice (0/5) showed any signs of abnormality in the bladder tissue after 3 or 5 months (Figs. 1C and 1D).

Ex vivo real-time multispectral imaging of BC in BBN-induced mouse model

We used the *ex vivo* organ culture to evaluate the suitability of the new real-time multispectral imaging in the preclinical mouse model, based on the report for the *ex vivo* detection of human bladder tumour tissue by the CD47 antibody [12]. Excised mouse bladders were prepared as described in the Materials and Methods section and incubated with Hexaminolevulinat (HAL, Hexvix®), CD47-FITC, CD90.2-FITC or a combination of CD90.2-FITC/ CD47-FITC and HAL, along with bladders from mock-treated control mice. The selection of the chemicals was based on the application in human BC imaging (HAL) or their reported expression in human BC [12–14]. Fig. 2A shows images of murine bladders recorded with the multispectral imaging system, which allows simultaneous imaging of the white light reflectance and the fluorescence
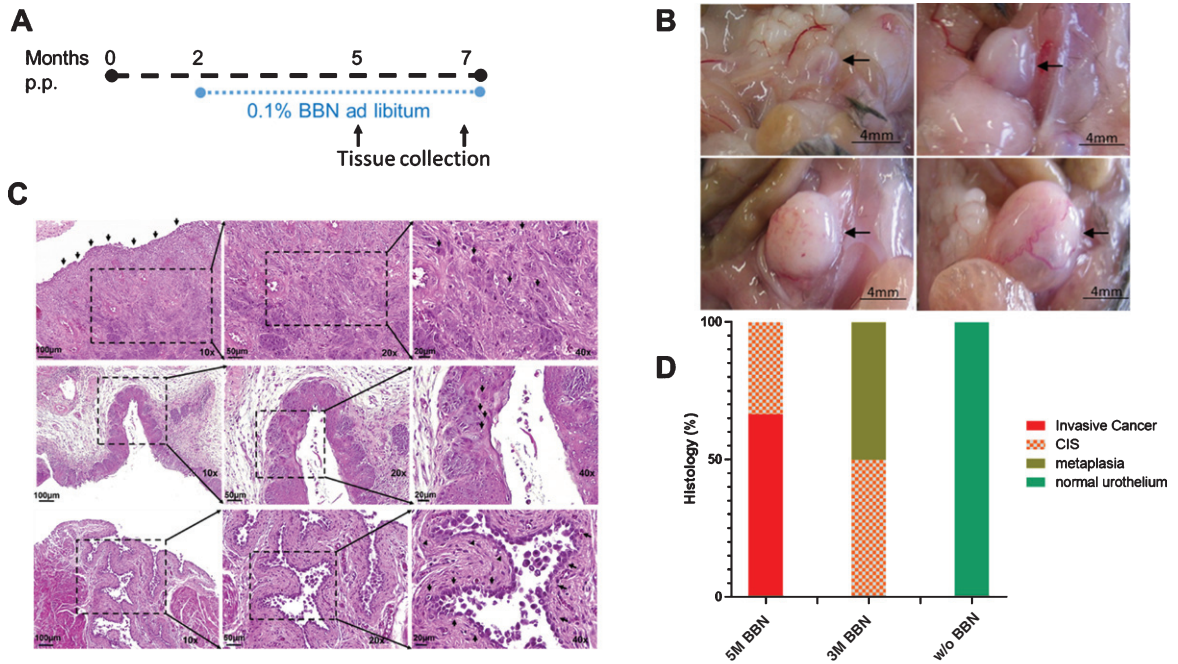
Fig. 1. BBN-induced bladder cancer recapitulates human bladder cancer. (A) Schematic representation of the BBN-induced bladder cancer model. Male mice with C57BL/6 genetic background were obtained from Janvier Labs at the age of 6 weeks. Starting at the age of 8 weeks, they received 0.1% BBN *ad libitum* in drinking water, which was freshly prepared every week. After 3 or 5 months of treatment (at the age of ∼20 or ∼28 weeks, respectively) the mice were sacrificed, and the bladders were excised for microscopy. (B) Macro-view of mouse bladders. (Top left) no BBN treatment; normal bladder; pathological result: normal bladder. (Top right) BBN treatment for 5 months; enlarged bladder; pathological result: squamous CIS with focal invasion. (Bottom left) BBN treatment for 5 months; enlarged bladder; pathological result: squamous carcinoma. (Bottom right) BBN treatment for 5 months; enlarged bladder; high vascularization; pathological result: squamous CIS. (C) Histological evaluation of normal and tumour mouse bladder tissues. (Top row) Representative images of a BBN induced carcinoma of a murine bladder. Black arrows highlight the superficial urothelial lining. Carcinoma infiltrates show an undermining growth pattern (marked area). Higher magnifications (right panel) show poorly differentiated carcinoma cells with highly pleomorphic and atypical nuclei with prominent nucleoli as well as prominent intercellular bridges resembling a feature of squamous differentiation (representative atypical nuclei are marked with black arrows). Keratinization is not present. (Middle row) Urothelial lining of a BBN murine bladder with prominent squamous metaplasia with focal high-grade atypia (marked area). In the 40× magnification (right panel) the metaplastic cells show marked high-grade atypia with pleomorphic nuclei and disturbed epithelial architecture (representative atypical nuclei are marked with black arrows). (Bottom row) Normal urothelial lining without squamous metaplasia or dysplasia. Urothelial cells are marked with black arrows. (D) Graphical illustration of the histological evaluation of mice tissues. H&E staining, followed by pathologic analysis, were conducted with 30 BBN-induced bladder tumours. 5M and 3M stand for 5 months and 3 months, respectively. The detailed information on tissue histology is depicted in Table I. Please note that invasive cancer comprises all samples with invasion of the submucosal tissue layer or the muscularis propria, i.e. all carcinoma and CIS with focal invasion.

of multiple fluorophores. The bladders were treated with HAL, a substrate of the heme metabolism that is metabolized to protoporphyrine IX (PpIX) and accumulates in cancer cells [20–22]. The PpIX fluorescence is excited at 405 nm, and it fluoresces in the red region of the visible spectrum (peak of the fluorescence emission at 635 nm). The red fluorescence can be detected predominantly in the bladder samples of the five months BBN-treated mice (Fig. 2A, middle column, indicated by arrows). Of note, the white light reflectance of these tissues indicates strong proliferation/hyperplasia compared to the mock-treated controls or the 3 months BBN-treated mice (Fig. 2A,

left column), in line with tumour detection of human BC by white light as indicated above. This observation is also supported by the histological evaluation, which shows invasive carcinoma or CIS for these samples (Table 1).

The elevated PpIX is also seen in the image showing the ratio between the unmixed PpIX signal and the autofluorescence/background signal (BGD signal) (Fig. 2A, right column). The high PpIX signal of the 5 months BBN-treated murine bladders is depicted in Fig. 2B, which shows the median ratio between the median PpIX signal and the median background signal. Bladders of 5 months BBN-treated mice ($n = 20$)

show a significantly higher PpIX signal/BGD ratio compared to all other groups (Fig. 2B, first group: +BBN, 5M + HAL). Histological analysis of the mouse bladders shown in Fig. 1C revealed invasive carcinoma and CIS, which is in good agreement with the clear positive PpIX fluorescence signal (Table 1).

As expected, all 5 months BBN-treated bladders ($n = 4$), which were not stained with HAL were negative for the PpIX signal (Fig. 2A–D: +BBN/–HAL), indicating the specificity of HAL-signal for tumour tissue. The weak PpIX/BGD signals in these –HAL control mice (Fig. 2A, bottom row) can be discrim-
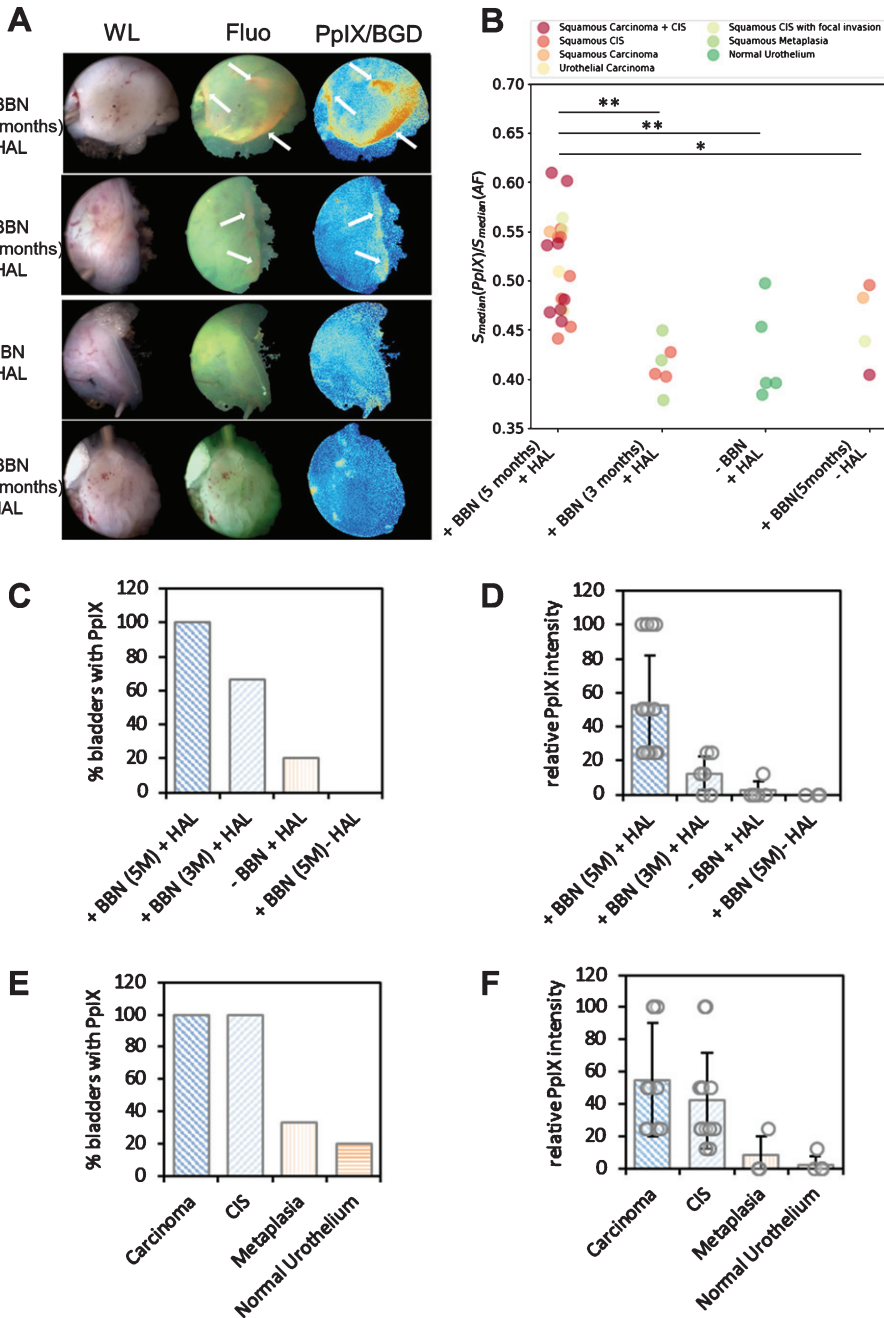

Fig. 2. (*Continued*).

Fig. 2. *Ex vivo* real-time multispectral imaging of BC in BBN-induced mouse model. (A) Endoscopic images of excised murine bladders under BBN treatment acquired by the multispectral camera system. Image modes: WL: white light, Fluo: fluorescence, PpIX: unmixed PpIX fluorescence channel and ratio PpIX/BGD:The ratio between the unmixed PpIX signal and the unmixed autofluorescence/FITC (BGD) signal. (Colormap: Blue = low values, Orange/Red = high values). Arrows indicate the PpIX signal. (B) Category plot of the ratio between the unmixed PpIX signal and the unmixed autofluorescence/FITC signal per murine bladder. The ratio describes a coarse measure of the overall presence of PpIX in the investigated murine bladders. Labels show the pathological staging of the murine bladders. Mann-Whitney-U-Test was used for statistical analysis (*$p < 0.05$, **$p < 0.005$). (C) Bar plot showing the percentage of bladders with positive PpIX signals on visual inspection of the processed videos. The different treatment categories are indicated. 5M = 5 months, and 3M = 3 months, respectively. (D) Subjective rating of PpIX signal intensity per bladder (= relative PpIX signal intensity). The signal intensity of a bladder was rated with 1.0 for a strong signal, with 0.5 for a moderate signal, 0.25 for a weak signal and with 0.125 for very weak signal and 0 for no signal (see also Table I). Bars show mean +/– standard deviation. The sum of all ratings per category was divided by total mouse number in each category and multiplied by 100 to calculate the arbitrary values. The different treatment categories are indicated. 5M = 5 months, and 3M = 3 months, respectively. (E) Bar plot showing the percentage of bladders with positive PpIX signal on visual inspection of the processed videos. Histological results shown in B were pooled as follows: Carcinoma (Squamous Carcinoma + CIS, Squamous Carcinoma, Urothelial Carcinoma), CIS (Squamous CIS, Squamous CIS with focal invasion), Metaplasia (Squamous Metaplasia), Normal Urothelium. –HAL bladders were excluded. (F) Subjective rating of PpIX signal intensity per bladder (= relative PpIX signal intensity). The signal intensity of a bladder was rated with 1.0 for a strong signal, with 0.5 for a moderate signal, 0.25 for a weak signal and with 0.125 for very weak signal and 0 for no signal (see also Table 1). Bars show mean +/– standard deviation. The sum of all ratings per category was divided by total mouse number in each category and multiplied by 100 to calculate the arbitrary values. The different treatment categories are indicated. 5M = 5 months, and 3M = 3 months, respectively.

inated from the true PpIX-positive signal observed in +BBN(5M)/+HAL and +BBN(3M)/+HAL mice in the white light image and fluorescence image. The quantitative evaluation of these signals in the +BBN/–HAL-group clearly indicates them as false-positive when compared to the +BBN (5M)/+HAL group (Fig. 2C, D).

Notably, the 3 months BBN-treated mouse bladder (+BBN(3M)/+HAL) presented in Fig. 2A shows a positive PpIX signal in the peripheral region in the fluorescence image (Flou) as well as in the ratio (PpIX/BGD). At the same time, the bladder tissue of the BBN-untreated control mouse is PpIX-negative (Fig. 2A, second row, indicated by an arrow). Local positive PpIX signals were observed in 4 out of 6 mice in this group (histologically defined as CIS or metaplasia), but a weak, non-specific PpIX-signal was observed only in one of the five –BBN/+HAL mice and in none of the mock-treated control mice (Fig. 2C, 2D and Table 1). Please note that the ratio between PpIX and background of the 3 months BBN-treated group is not significantly different from the control groups, probably due to the overall negative signals, damping the specific signal values in the total calculation (Fig. 2B). These results suggest that local, premalignant lesions can be detected with the new imaging system combined with HAL. In fact, the evaluation of the results in relation to histology reveals that bladders of all mice with carcinoma (SCC and UCB) or CIS (CIS with or without local invasion) show a PpIX signal in the fluorescence image (Fig. 2E). Moreover, the relative PpIX signal intensity of the bladders with carcinoma and CIS is elevated compared to the bladders

with metaplasia or normal urothelium (Fig. 2F). In fact, also the bladders with metaplasia exhibit slightly higher signal intensities compared to healthy bladders (∼8 versus ∼2,5, Fig. 2F), though the signal intensities vary significantly among individual samples.

In summary, distinct PpIX signals were detected in the bladder tissue of all ($n = 20$) of the 5 months BBN-treated mice incubated with HAL (Fig. 2C, D). Moreover, the relative PpIX signal intensity was the highest (52.5) in this group (Fig. 2D, and Table 1), whereas only one of the five control mouse bladders incubated with HAL (–BBN/+HAL) showed weak, false-positive PpIX fluorescence (relative PpIX signal intensity 2.5). Importantly, although the average signal intensities of the 3 months BBN-treated mice (3 months BBN/+HAL) were comparable to the control groups (–BBN/+HAL and +BBN/–HAL), they showed specific local signals, in line with early lesions observed in this group (CIS or metaplasia). Interestingly, PpIX signal intensity shows some degree of variation within the same group (i.e. histology) (Table 1), potentially due to the localization of the degenerated tissue.

Fluorescence imaging shows that the staining with FITC-conjugated antibodies against surface proteins CD47 and CD90.2 is inconspicuous. A FITC-signal could not be detected with bladders labelled with FITC-conjugated antibodies against CD47. Some of the CD90-labelled bladders showed a FITC signal in the peripheral areas, especially the one incubated with higher antibody concentrations. Similarly, strong green autofluorescence was observed in all bladders, comparable to signals observed with CD90.2-FITC

and CD47-FITC antibodies, indicating that these antibodies had limited ability to detect BC in BBN-treated mice.

DISCUSSION

Currently, white light cystoscopy is the gold standard for initial BC diagnosis. New optical imaging technologies may improve BC detection and characterization, and the quality of transurethral resection. While data on photodynamic diagnosis are the strongest, clinical effectiveness of these technologies is not proven. Prospective studies are needed, particularly of narrow-band imaging, confocal laser endo-microscopy and optical coherence tomography. The suitability of new technologies for cystoscopy must be assessed in preclinical studies. Recently, we presented a novel multispectral imaging system for simultaneous fluorescence-guided real-time surgery [10]. We also demonstrated the application of the multiparametric cystoscopy on human bladder tumours [11]. In the present study, we used the established BC mouse model to evaluate the new real-time multispectral imaging device in a preclinical model. Generally, male C57BL/6 mice are treated in this animal model, and macroscopic lesions arise at about the fifth month of BBN administration. Our results for the 5 months BBN-treatment group are in line with previous reports: the tumours are mostly invasive squamous cell carcinoma (SCC), reflecting the human SCC subgroup of human BC [17, 23]. The fact that we observe squamous metaplasia at early phases but not urothelial CIS indicates that the tumours are true SCCs but not urothelial carcinoma with squamous differentiation. Irrespective of the tumour subtype, in combination with HAL (hexylaminolevulinate), we could detect specific PpIX signals from all tumours with the new imaging device indicating the suitability of the new rMSI for BC detection. A differentiation between the different pathological stages of tumours was possible, although PpIX signal intensity shows some degree of variation within the same group (Table 1). Especially, carcinoma and CIS could be well differentiated from metaplasia and healthy urothelium. However, the main advantage of rMSI lies in the capability to detect multiple fluorophores concurrently with the white light image. In this respect, the two antibodies used in this study (CD47 and CD90.2) did not prove to be specific for can-

cer cell detection. Although these antibodies were described to recognize tumour cell antigens, this observation was reported for human urothelial carcinoma of the BC [12–14]. Likely, these markers are not expressed in the mouse SCC subtype. We could not detect these markers in initial expression analyses (not shown). We currently determine the expression of surface markers in the BBN-induced mouse SCCs for their application for rMSI in the future. Also, BBN-treatment of p53 heterozygous C57BL/6 mice induces a higher frequency of BC [23]. This mouse model could be potentially better suited for urothelial cancer of the bladder. While we were not able to image the FITC-labelled antibodies with the rMSI system most probably due to lack of the targeted proteins on the cancer cell surface, our novel endoscopic device allowed in combination with HAL detection of premalignant conditions of the bladder epithelium, CIS and, to some extent, metaplastic degeneration of the bladder tissue. Of note, although the exact time-period of CIS evolution and the progression to invasive tumours cannot be predicted, it seems reasonable to assume that mice treated for 3 to 4 month have a higher probability to have CIS, rather than invasive cancers. It may be therefore worth considering a 3–4 month BBN-treatment of mice for the evaluation of early tumour markers.

Taken together, the rMSI system allows the simultaneous detection of multiple fluorescent agents, including PpIX, the metabolite of Hexaminolevulinat (HAL, Hexvix®), in combination with the white light reflectance and provides the opportunity to merge these two modalities into a single image. This unique feature already demonstrates an advantage over the current endoscopic equipment used in daily clinical practice. For instance, with the new rMSI imaging system, the surgeon can see three images in parallel on the screen: the white light image, the PDD image and a merged image of these two. Thus, the malignant tissue can be detected and resected in the merged modality without any need to switch between blue light and white light. Moreover, due its sensitivity, the rMSI system allows the detection of early precursor lesions in the *ex vivo* experimental system. We aim to refine and extend these features for the detection of malignant lesions in humans *in vivo*, including early precursor lesions. In combination with tumour-specific molecular markers the system provides the opportunity to achieve a great diagnostic advancement. This would not only enable

the specific detection of tumour cells but also help to distinguish inflamed tissue from cancerous lesions, a current problem in HAL-based blue light cystoscopy.

ACKNOWLEDGMENTS

FUNDING

AUTHOR CONTRIBUTIONS

CG, CB, ND (conception); SM, JR, XZ, ME, DH (performance of work); BG, MK (interpretation and data analysis); CG, SM, JR (writing of the article). All authors (critical reading of the manuscript).

CONFLICT OF INTEREST

Dr. Nikolaos C. Deliolanis is a co-inventor for multispectral imaging patent applications. Dr. Nikolaos C. Deliolanis and Dr. Bartłomiej Grychtolis are co-founders of Thericon GmbH. The remaining authors have nothing to disclose.

REFERENCES

[1] Antoni S, Ferlay J, Soerjomataram I, Znaor A, Jemal A, Bray F. Bladder Cancer Incidence and Mortality: A Global Overview and Recent Trends. Eur Urol. 2017;71(1):96-108.

[2] Wong W, Yim YM, Kim A, Cloutier M, Gauthier-Loiselle M, Gagnon-Sanschagrin P, et al. Assessment of costs associated with adverse events in patients with cancer. PLoS One. 2018;13(4):e0196007.

[3] Babjuk M, Burger M, Zigeuner R, Shariat SF, van Rhijn BW, Comperat E, et al. EAU guidelines on non-muscle-invasive urothelial carcinoma of the bladder: update 2013. Eur Urol. 2013;64(4):639-53.

[4] Janisch F, Abufaraj M, Fajkovic H, Kimura S, Iwata T, Nyirady P, et al. Current Disease Management of Primary Urethral Carcinoma. Eur Urol Focus. 2019;5(5):722-34.

[5] Mari A, Abufaraj M, Gust KM, Shariat SF. Novel endoscopic visualization techniques for bladder cancer detection: a review of the contemporary literature. Curr Opin Urol. 2018;28(2):214-8.

[6] Kriegmair MC, Honeck P, Theuring M, Bolenz C, Ritter M. Wide-field autofluorescence-guided TUR-B for the detection of bladder cancer: a pilot study. World J Urol. 2018;36(5):745-51.

[7] Rink M, Babjuk M, Catto JW, Jichlinski P, Shariat SF, Stenzl A, et al. Hexyl aminolevulinate-guided fluorescence cystoscopy in the diagnosis and follow-up of patients with non-muscle-invasive bladder cancer: a critical review of the current literature. Eur Urol. 2013;64(4):624-38.

[8] Zheng C, Lv Y, Zhong Q, Wang R, Jiang Q. Narrow band imaging diagnosis of bladder cancer: systematic review and meta-analysis. BJU Int. 2012;110(11 Pt B):E680-7.

[9] Mayr R, Burger M. Value of fluorescence cystoscopy in high risk non-muscle invasive bladder cancer. Curr Urol Rep. 2013;14(2):90-3.

[10] Dimitriadis N, Grychtol B, Theuring M, Behr T, Sippel C, Deliolanis NC. Spectral and temporal multiplexing for multispectral fluorescence and reflectance imaging using two color sensors. Opt Express. 2017;25(11):12812-29.

[11] Kriegmair MC, Rother J, Grychtol B, Theuring M, Ritter M, Gunes C, et al. Multiparametric Cystoscopy for Detection of Bladder Cancer Using Real-time Multispectral Imaging. Eur Urol. 2020;77(2):251-9.

[12] Pan Y, Volkmer JP, Mach KE, Rouse RV, Liu JJ, Sahoo D, et al. Endoscopic molecular imaging of human bladder cancer using a CD47 antibody. Sci Transl Med. 2014;6(260):260ra148.

[13] Skowron KB, Pitroda SP, Namm JP, Balogun O, Beckett MA, Zenner ML, et al. Basal Tumor Cell Isolation and Patient-Derived Xenograft Engraftment Identify High-Risk Clinical Bladder Cancers. Sci Rep. 2016;6:35854.

[14] Volkmer JP, Sahoo D, Chin RK, Ho PL, Tang C, Kurtova AV, et al. Three differentiation states risk-stratify bladder cancer into distinct subtypes. Proc Natl Acad Sci U S A. 2012;109(6):2078-83.

[15] Akagi G, Akagi A, Kimura M, Otsuka H. Comparison of bladder tumors induced in rats and mice with N-butyl-N-(4-hydroxybutyl)-nitrosoamine. Gan. 1973;64(4):331-6.

[16] Bertram JS, Craig AW. Specific induction of bladder cancer in mice by butyl-(4-hydroxybutyl)-nitrosamine and the effects of hormonal modifications on the sex difference in response. Eur J Cancer. 1972;8(6):587-94.

[17] Fantini D, Seiler R, Meeks JJ. Molecular footprints of muscle-invasive bladder cancer in smoking and nonsmoking patients. Urol Oncol. 2019;37(11):818-25.

[18] Shin K, Lim A, Odegaard JI, Honeycutt JD, Kawano S, Hsieh MH, et al. Cellular origin of bladder neoplasia and tissue dynamics of its progression to invasive carcinoma. Nat Cell Biol. 2014;16(5):469-78.

[19] Vasconcelos-Nobrega C, Colaco A, Lopes C, Oliveira PA. Review: BBN as an urothelial carcinogen. *In Vivo*. 2012;26(4):727-39.

[20] Kennedy JC, Pottier RH, Pross DC. Photodynamic therapy with endogenous protoporphyrin IX: basic principles and present clinical experience. J Photochem Photobiol B. 1990;6(1-2):143-8.

[21] Lange N, Jichlinski P, Zellweger M, Forrer M, Marti A, Guillou L, et al. Photodetection of early human bladder cancer based on the fluorescence of 5-aminolaevulinic acid hexylester-induced protoporphyrin IX: a pilot study. Br J Cancer. 1999;80(1-2):185-93.

[22] Zenzen V, Zankl H. Protoporphyrin IX-accumulation in human tumor cells following topical ALA- and h-ALA-application *in vivo*. Cancer Lett. 2003;202(1):35-42.

[23] Van Batavia J, Yamany T, Molotkov A, Dan H, Mansukhani M, Batourina E, et al. Bladder cancers arise from distinct urothelial sub-populations. Nat Cell Biol. 2014;16(10): 982-91, 1-5.